RESEARCH ARTICLE | JULY 02 2015

Direct and phonon-assisted indirect Auger and radiative recombination lifetime in HgCdTe, InAsSb, and InGaAs computed using Green's function formalism

Hanqing Wen; Benjamin Pinkie ; Enrico Bellotti

J. Appl. Phys. 118, 015702 (2015)
https://doi.org/10.1063/1.4923059

JOURNAL OF APPLIED PHYSICS **118**, 015702 (2015)

Direct and phonon-assisted indirect Auger and radiative recombination lifetime in HgCdTe, InAsSb, and InGaAs computed using Green's function formalism

Hanqing Wen, Benjamin Pinkie, and Enrico Bellotti[a)]
Department of Electrical and Computer Engineering, Boston University, 8 Saint Mary's Street, Boston, Massachusetts 02215, USA

(Received 6 April 2015; accepted 16 June 2015; published online 2 July 2015)

Direct and phonon-assisted (PA) indirect Auger and radiative recombination lifetime in HgCdTe, InAsSb, and InGaAs is calculated and compared under different lattice temperatures and doping concentrations. Using the Green's function theory, the electron self energy computed from the electron-phonon interaction is incorporated into the quantum-mechanical expressions of Auger and radiative recombination, which renders the corresponding minority carrier lifetime in the materials due to both direct and PA indirect processes. Specifically, the results of two pairs of materials, namely, $InAs_{0.91}Sb_{0.09}$, $Hg_{0.67}Cd_{0.33}Te$ and $In_{0.53}Ga_{0.47}As$, $Hg_{0.38}Cd_{0.62}Te$ with cutoff wavelengths of 4 μm and 1.7 μm at 200 K and 300 K, respectively, are presented. It is shown that for $InAs_{0.91}Sb_{0.09}$ and $Hg_{0.67}Cd_{0.33}Te$, when the lattice temperature falls below 250 K the radiative process becomes the limiting factor of carrier lifetime in both materials at an *n*-type doping of $10^{15}\,cm^{-3}$, while at a constant temperature of 200 K, a high *n*-type doping ($N_D > 5 \times 10^{15}\,cm^{-3}$ for $InAs_{0.91}Sb_{0.09}$ and $3 \times 10^{15}\,cm^{-3}$ for $Hg_{0.67}Cd_{0.33}Te$) makes the Auger process dominate. For the Auger lifetime in $In_{0.53}Ga_{0.47}As$ and $Hg_{0.38}Cd_{0.62}Te$, the calculation suggested that under all the temperatures and *n*-doping concentrations investigated in this paper, radiative process is always the limiting factor of the materials' minority carrier lifetime. The calculation of the PA indirect Auger process in the four materials further demonstrated its indispensable contribution to the materials' total Auger rate especially at low temperature, which is necessary to reproduce some experimental data. By fitting the Beattie-Landsberg-Blakemore (BLB) formula to the numerical Auger results, the corresponding overlap integral factors $|F_1F_2|$ in BLB theory are evaluated and presented to facilitate fast and accurate Auger calculations in the IR detector simulations. [http://dx.doi.org/10.1063/1.4923059]

I. INTRODUCTION

Aiming to operate the next-generation infrared (IR) detectors at higher temperature with improved quantum efficiency over a wide spectral range, especially in the mid-wavelength IR (MWIR) and short-wavelength IR (SWIR) band, the detector community has proposed many novel detector architectures. Among them are barrier detectors, normally referred to as XBn[1–3] and photon-trapping structures[4,5] which exhibit high quantum efficiency, reduced crosstalk and low dark current compared to the conventional planar detectors.[6] A prerequisite to realize these novel detector structures with potentially superior performance is to understand the properties of the materials to be employed and how they influence the device operation. Of all the established and emerging narrow band-gap semiconductors, special consideration has been given to the lattice matched (LM) III–V ternary alloys. Specifically Indium Arsenide Antimonide (InAsSb), which is LM to Gallium Antimonide (GaSb), and Indium Gallium Arsenide (InGaAs) LM to Indium Phosphide (InP) have been employed alongside Mercury Cadmium Telluride (HgCdTe) for detector applications in the MWIR and SWIR spectral regions, respectively. Although, it is important to design and optimize the structure of a specific detector to exploit the unique features of a given material, the mechanisms that determine the intrinsic minority carrier lifetime impose a fundamental limit to the device performance.[7]

Unlike extrinsic carrier recombination mechanisms, such as Shockley-Read-Hall (SRH) recombination, that can be reduced by improving the material quality, Auger and radiative recombination processes are closely related to the details of the material's electronic structure and therefore are more difficult to engineer. As a result, comparing the intrinsic minority carrier lifetime of these narrow-gap III–V alloys with the widely used HgCdTe is important to understand the potential advantages of one specific material over the other for a given detector application.

A number of theoretical and experimental investigations have been performed to study Auger and radiative recombination processes and the minority carrier lifetime in HgCdTe, InAsSb, and InGaAs. In particular, Krishnamurthy *et al.*[8] and Grein *et al.*,[9] respectively, employed the hybrid pseudopotential tight binding and a 14-band $k \cdot p$ band structure and calculated the direct Auger and radiative lifetime in HgCdTe using Fermi's golden rule. With a similar formalism, Bertazzi *et al.*[10] used band structures from the empirical pseudopotential method (EPM) and obtained comparable

a)Electronic mail: bellotti@bu.edu

results for direct Auger-1 and Auger-7 lifetime in $Hg_{0.78}Cd_{0.22}Te$.

In the case of InAsSb alloys, the study of Auger recombination processes has been performed for superlattice structures.[11–13] Specifically, Grein *et al.*[14] theoretically compared the performances of type-II InAs/InGaSb superlattices to the conventional HgCdTe detectors operating at long wavelength IR (LWIR) using the $k \cdot p$ method and found that InAsSb-based detectors outperformed their HgCdTe-based counterparts due to their smaller Auger recombination rates. Vinter[15] calculated the direct Auger coefficients in InAs, InSb and $InAs_{1-x}Sb_x$ alloys in both bulk materials and superlattices with an extended $k \cdot p$ band structures, where the results showed a good agreement with the experimental data at 300 K. This indicated that the direct Auger process is the dominant Auger recombination mechanism at this temperature, but similar information at other temperatures in these materials is still missing. As to InGaAs alloys, the majority of the studies of their Auger recombination have been performed using the parabolic band approximation[16–18] to investigate their applications in lasers and high-speed photodetectors. However, except for some early works based on analytical models,[16,17] few studies have focused on the phonon-assisted (PA) indirect Auger process which is believed to be important in InGaAs alloys.[16] In fact, it is still unclear whether PA indirect processes are important to understand the Auger and radiative properties in InGaAs especially with full-band structure based models, where the total density of states is different than that obtained from analytical bands.

The main goal of this works is to perform a comparative study of the Auger and radiative recombination properties of InGaAs, InAsSb, and HgCdTe to highlight potential advantages of one material system with respect to the others at given operating conditions. In this work, both direct and PA indirect Auger as well as the radiative recombination processes are investigated using the Green's function formalism.[19,20] Full band structures of each alloys, that are obtained using EPM, are also employed to overcome the limitations of analytical non-parabolic bands, leading to a more accurate evaluation of the interaction matrix element.[21,22] By using the Green's function formalism, the treatment of the divergences that appear in the second-order perturbation theory (SOPT) can be naturally avoided and the full band structure, as a result, can be incorporated into the calculation without *ad-hoc* approximations.[19,20]

The work will first focus on the LWIR spectral range and present the calculated Auger lifetime for $Hg_{0.78}Cd_{0.22}Te$ to compare the results to other numerical models. Subsequently, we performed a detailed comparison of both Auger and radiative lifetime in two sets of material compositions: $InAs_{0.91}Sb_{0.09}$ and $Hg_{0.67}Cd_{0.33}Te$ intended for detector operation in the MWIR and $In_{0.53}Ga_{0.47}As$ and $Hg_{0.38}Cd_{0.62}Te$ for SWIR, which have cutoff wavelengths of 4 μm and 1.7 μm at 200 K and 300 K, respectively. Finally, the corresponding overlap integral factor $|F_1F_2|$ that are needed to evaluate the Auger rates using the Beattie-Landsberg-Blakemore (BLB) expression will also be derived by fitting the theoretical formula to the numerical Auger coefficients. This will make it possible to set up a fast and accurate Auger recombination rate evaluation for device simulations.

The manuscript is organized as follows: Sec. II will outline the theoretical approach and the numerical implementation employed in this work. Section III will discuss the results obtained for HgCdTe, InAsSb, and InGaAs, and it will highlight the relative importance of both direct and PA indirect Auger recombination as a function of lattice temperatures and doping concentrations. Finally, Sec. IV will deliver the concluding remarks.

II. THEORY AND NUMERICAL IMPLEMENTATION

A. Auger recombination

The theoretical aspects of both direct (also called "pure-collision") and PA indirect Auger recombination processes have been studied and developed since 1960s when Beattie[23] first proposed an analytical expression, known as BLB formula, to compute the Auger coefficient under the approximation of parabolic band structure and non-degenerate statistics. Though the BLB formula is a convenient way to estimate the Auger lifetime in direct band gap material and therefore is still widely adopted in the device simulation nowadays, the calculated rates, on the other hand, heavily depend on the value of overlap integral factor $|F_1F_2|$, which is historically chosen between 0.1 and 0.3 without any clear guidelines. While recent calculations[9] based on a 14-band $k \cdot p$ band structure indicated that the overlap integral factor should be closer to the lower bound of its supposed range to match the numerical results, the actual value of $|F_1F_2|$ remains a fitting parameter. As a result, to eliminate the ambiguity of evaluating Auger coefficient, a first-principle systematic approach to compute the recombination process is highly desirable.

At present, perhaps the most rigorous Auger recombination theory is the one that was developed by Takeshima[17] and Bardyszewski and Yevick[16] who incorporated both direct and indirect (e.g., phonon-assisted and impurity assisted) processes into the Green's function formalism to enhance the accuracy of the model. Although a parabolic band approximation was used in these early works due to the limitation of the computing infrastructure, the formalism itself is amenable to the use of a full band structure of the material being studied, which is particularly important to increase the accuracy of the calculation when the carriers' energy levels are far from the Γ point.[20] It is worthy of note that, besides the Green's function theory, SOPT is also widely employed in studying the indirect Auger process.[24] However, due to the undefined behavior of the SOPT equation when a virtual state overlaps with a real one, the theory's numerical accuracy has been questioned,[17,25] especially when a full band structure is used. To avoid this difficulty, in this work, we followed the procedure proposed by Takeshima[17,18] and implemented the Green's function theory of Auger recombination with full band structures obtained from EPM. A detailed derivation of the expression for the recombination rates was presented in Ref. 17 and will not be repeated here.

The resulting total Auger recombination rate per unit volume in bulk material is given by

$$R_{\mathrm{AR}} = \frac{2\pi}{\hbar}\frac{V^3}{(2\pi)^9}[1-e^{(\mu_v-\mu_c)/k_BT}]\int\int\int\int \mathrm{d}\mathbf{k}_1\mathrm{d}\mathbf{k}_2\mathrm{d}\mathbf{k}_{1'}\mathrm{d}\mathbf{k}_{2'} \times |M_{ee}|^2\delta(\mathbf{k}_1+\mathbf{k}_2-\mathbf{k}_{1'}-\mathbf{k}_{2'}) \times \int \mathrm{d}E_1\mathrm{d}E_2\mathrm{d}E_{1'}\mathrm{d}E_{2'}\Theta(E_1)\Theta(E_2)[1-\Theta(E_{1'})] \times [1-\Theta(E_{2'})]\times \mathrm{Im}G^R_{l_1}(\mathbf{k}_1,E_1)\mathrm{Im}G^R_{l_2}(\mathbf{k}_2,E_2) \times \mathrm{Im}G^R_{l_{1'}}(\mathbf{k}_{1'},E_{1'})\mathrm{Im}G^R_{l_{2'}}(\mathbf{k}_{2'},E_{2'}), \quad (1)$$

where $\mathrm{Im}G^R_{l_i}(\mathbf{k}_i,E_i)$ is the spectral density function representing the energy broadening at $\mathbf{k}_i$ in Brillouin Zone (BZ) around energy E_i at band l_i. The specific form of the expression can be found in Sec. II C. M_{ee} is the matrix element for Auger process which involves four electron/hole states[21]

$$M_{ee} = \int\int \mathrm{d}\mathbf{r}_1\mathrm{d}\mathbf{r}_2\phi^*_{\mathbf{k}_1}(\mathbf{r}_1)\phi^*_{\mathbf{k}_2}(\mathbf{r}_2)\nu(\mathbf{r}_1-\mathbf{r}_2) \times \phi_{\mathbf{k}_{1'}}(\mathbf{r}_1)\phi_{\mathbf{k}_{2'}}(\mathbf{r}_2) + \text{exchange term}, \quad (2)$$

with

$$\phi_{\mathbf{k}}(\mathbf{r}) = \frac{1}{\sqrt{V}}\sum_{\mathbf{G}}[A_u(\mathbf{k}+\mathbf{G})+A_d(\mathbf{k}+\mathbf{G})]e^{i(\mathbf{k}+\mathbf{G})\cdot\mathbf{r}}, \quad (3)$$

$$\nu(\mathbf{r}) = \sum_{\mathbf{G}}\int_{\mathrm{BZ}}\frac{\mathrm{d}\mathbf{q}}{(2\pi)^3}\nu(\mathbf{q}+\mathbf{G})e^{i(\mathbf{q}+\mathbf{G})\cdot\mathbf{r}}, \quad (4)$$

$$\nu(\mathbf{q}+\mathbf{G}) = \sum_{\mathbf{G}'}\epsilon^{-1}_{\mathbf{G},\mathbf{G}'}(\mathbf{q})\frac{4\pi e^2}{|\mathbf{q}+\mathbf{G}'|^2}. \quad (5)$$

Here, V is the volume of the crystal and $\phi_{\mathbf{k}}(\mathbf{r})$ is the Bloch wavefunction whose plane wave expansion coefficients are $A_u(\mathbf{k}+\mathbf{G})$ and $A_d(\mathbf{k}+\mathbf{G})$ for spin up and spin down states, respectively.[22] $\epsilon^{-1}_{\mathbf{G},\mathbf{G}'}(\mathbf{q})$ is the dielectric function of the material and $\nu(\mathbf{r})$ is the screened Coulomb interaction. The exchange term in Eq. (2) can be obtained by swapping the indices $1'$ and $2'$ in the direct term. When using plane waves to expand the electron wavefunction $\phi_{\mathbf{k}}(\mathbf{r})$, the overlap integral of the four Bloch states involves a four-fold summation over the reciprocal vector $\mathbf{G}$. Due to the large number of plane waves used in the EPM, direct summation over $\mathbf{G}$ is very time consuming. Since the interaction matrix element needs to be evaluated very frequently during the calculation of Auger rate, we followed the approach of Laks and Neumark[21] and reduced the four-fold summation into a two-fold one which greatly decreased the computing requirement. It should be noted that since Auger process is mediated by the electron-electron interaction, the screening of the electric field due to electron gas plays a vital role in modeling the interaction. Therefore, in this work, we employed a wavevector-dependent dielectric function $\epsilon(\mathbf{q})$ to account for the spatial screening effect

$$\epsilon(\mathbf{q}) = 1+\frac{c_1}{|\mathbf{q}|^{c_2}+c_3}, \quad (6)$$

with the parameters c_1, c_2, and c_3 fitted to the numerical results from the random phase approximation.[26] We want to point out that a more rigorous way of modeling the screening effect in Auger process is to further include the frequency dependence in the dielectric function. However, due to the significant increase of computing time, the dynamic screening effect is hard to incorporate with full band structure and as a result, only wavevector-dependent screening is considered in this work.

Having the total Auger recombination rate, Auger coefficients C_n, C_p and minority carrier lifetimes τ^{AR} under low injection condition can be obtained as

$$R_{\mathrm{AR}} = (C_n n + C_p p)(np - n_i^2), \quad (7)$$

$$\tau^{\mathrm{AR}} = \frac{n_i^2}{R_{\mathrm{AR}}(n_0+p_0+\Delta)}, \quad (8)$$

where n_i, n_0, p_0, and Δ are the intrinsic, electron, and hole concentrations at thermal equilibrium and injected carrier concentration, respectively.

To facilitate the calculation of the overlap integral in the BLB formula, the corresponding n-type Auger coefficient C_n is cited as the following:[27]

$$C_n = \frac{\left(\frac{m_e^*}{m_0}\right)|F_1F_2|^2}{7.6\times10^{-18}n_i^2\epsilon_\infty^2\left(1+\frac{m_e^*}{m_h^*}\right)^{1/2}\left(1+2\frac{m_e^*}{m_h^*}\right)} \times\left(\frac{E_g}{k_BT}\right)^{-3/2}\exp\left[-\frac{1+2\frac{m_e^*}{m_h^*}}{1+\frac{m_e^*}{m_h^*}}\cdot\frac{E_g}{k_BT}\right], \quad (9)$$

with m_e^*, m_h^*, ϵ_∞, E_g, and $|F_1F_2|$ being the electron and hole effective masses, high-frequency dielectric constant, band gap energy, and overlap integral factor, respectively. Except for $|F_1F_2|$, the empirical formulas of these quantities as a function of composition ratio and temperature can be found in Refs. 3, 28, and 29.

B. Radiative recombination

To describe the radiative recombination process, a similar expression for the rate can be derived from Green's function theory as well. The derivation of the formula including the corresponding phonon perturbed self energy function has been presented in detail in Ref. 20. Unlike the Auger process, radiative electron-hole recombination is mediated by a dipole interaction, where a photon is emitted or absorbed to maintain the energy conservation. As a result, only two electron self energy functions present in the equation, which, respectively, account for the broadening of initial and final states under the electron-phonon interaction

$$R_{21}(\hbar\omega_{\mathrm{ph}}) = \frac{2e^2n_r\omega_{\mathrm{ph}}}{\pi\hbar m_0^2c_0^3V\epsilon_0}\sum_{\mathbf{k}_c,\mathbf{k}_v}|\langle\mathbf{k}_v|\hat{\mathbf{e}}\cdot\mathbf{P}|\mathbf{k}_c\rangle|^2 \times\int\mathrm{d}E_1'\int\mathrm{d}E_2'\Theta(E_2')(1-\Theta(E_1')) \times\delta(\mathbf{k}_c-\mathbf{k}_v-\mathbf{k}_{\mathrm{ph}})\delta(\mu_c-\mu_v+E_2'-E_1'-\hbar\omega_{\mathrm{ph}}) \times\mathrm{Im}G^R_{l_v}(\mathbf{k},E_1')\mathrm{Im}G^R_{l_c}(\mathbf{k},E_2'). \quad (10)$$

Here, e, m_0, ω_{ph}, $\mathbf{k}_{ph}$, ϵ_0, and $\hat{\mathbf{e}}$ are the electron charge and mass, frequency and momentum of photon, vacuum permittivity, and polarization of the photon, respectively. $\mathbf{P}$ is the momentum operator for dipole interaction, and $\Theta(E)$ is the Fermi factor defined as $\Theta(E) = 1/[1 + e^{E/(k_BT)}]$, where the energy E is measured from the corresponding quasi-Fermi level. Similar to the Auger process, the minority carrier lifetime due to radiative recombination under low injection condition is defined as

$$\tau^{RR} = \frac{n_i^2}{R_{21}(n_0 + p_0 + \Delta)}. \quad (11)$$

C. Spectral function and self energy

The core idea of Green's function theory lies in the fact that all the effects of perturbations (e.g., phonon and impurity scattering) can be expressed by expanding the system's self energy function using Dyson's equation.[30] Without repeating the similar procedure published in the literature,[17,20,30] the lowest order in the expansion which is usually sufficient to study the Auger and radiative recombination under low injection conditions is recorded below as a reference

$$\mathrm{Im}G_{l_i}^R(\mathbf{k}, E) = -\frac{1}{\pi} \times \frac{\mathrm{Im}\Sigma_i(\mathbf{k}, E)}{\left[E - E_i(\mathbf{k}) - \mathrm{Re}\Sigma_i(\mathbf{k}, E)\right]^2 + \left[\mathrm{Im}\Sigma_i(\mathbf{k}, E)\right]^2}, \quad (12)$$

and

$$\begin{aligned}\mathrm{Im}\Sigma_i(\mathbf{k}, E) = &-\pi \sum_\nu \int \frac{d\mathbf{k}'}{(2\pi)^3} |g_\nu(\mathbf{k}' - \mathbf{k})|^2 B_{ii}(\mathbf{k}, \mathbf{k}') \\ &\times \{[1 + P(\hbar\omega_\nu) - \Theta(E - \hbar\omega_\nu)] \\ &\times \delta(E - \hbar\omega_\nu - E_i(\mathbf{k}')) + [P(\hbar\omega_\nu) \\ &+ \Theta(E + \hbar\omega_\nu)]\delta(E + \hbar\omega_\nu - E_i(\mathbf{k}'))\}, \quad (13)\end{aligned}$$

where $B_{ii}(\mathbf{k}, \mathbf{k}')$ is the overlap integral between the periodic part of Bloch states with wave vectors $\mathbf{k}$ and $\mathbf{k}'$. The matrix elements $g_\nu(\mathbf{k}' - \mathbf{k})$ here represent four carrier-phonon interaction mechanisms, namely, acoustic, piezoelectric, non-polar optical, and polar optical interaction and their expression are summarized in Refs. 16 and 20. The phonon occupation factor $P(\hbar\omega_\nu)$ is given by the Bose-Einstein distribution, which is $P(\hbar\omega_\nu) = 1/[e^{\hbar\omega_\nu/(k_BT)} - 1]$.

D. Numerical implementation

The integration over the full BZ in Eqs. (1) and (10) is performed by discretizing the k-space using a band-adaptive tetrahedron mesh.[19] Specifically, tetrahedral meshes with 1672 and 2202 vertices in the irreducible wedge are used in the calculation of Auger and radiative recombination, respectively. Since most of the Auger and radiative recombination happens around the band edge under the low injection condition, in order to accommodate the band structure details while maintaining a reasonable computation time, the tetrahedral mesh is refined so that a large portion of vertices locate near the Γ valley. In fact, in the mesh we generated, almost 40% vertices are in a sphere with radius of $0.08\frac{2\pi}{a_0}$ centered at the Γ point, where a_0 denotes the lattice constant.

The most challenging aspect of calculating the Auger recombination rate lies in the four-fold three-dimensional integral over BZ in Eq. (1). Although the momentum conservation and energy conservation can eliminate four of the k-integration dimensions, the remaining eight integrals make the common numerical integration method infeasible in this case. As a result, we employed a Monte-Carlo integration technique for the first six-fold integral in k-space which represent the two initial states, and a finite-element integration method for the remaining two- or three-fold integral depending on whether the phonon perturbation is included or not. The convergence of the calculation is then tested with several pseudo-random number series, and the difference of the results between each run is less than 10%.

Since only direct gap semiconductors are considered in this work, the contribution of the PA indirect process to the radiative recombination, which is overwhelmed by the direct vertical transitions, is not important. Therefore in Eq. (10), the two spectral functions are substituted by two delta functions to simplify the calculation. As to the Auger process, due to the fact that most of the recombination events involve electron states that have large momentum difference, the number of available direct recombination paths is limited. On the other hand, when considering the PA process, the available final states in Auger recombination increase substantially which compensates its weak interaction strength. Consequently, in order to better understand the total Auger recombination in the materials it is necessary to take the phonon perturbation effect into consideration. It should be noted, however, that due to the complexity of the energy integral in Eq. (1), in our calculation of PA process only one band is broadened by using the actual spectral function. The rest of Green's functions are set to be delta functions. Since the heavy hole (HH) band usually has a larger broadening compared to that of the conduction bands, only the spectral function for this band is computed and included in Eq. (1).[18] To calculate the direct Auger process, we set all the spectral functions to be delta functions, and Eq. (1) will reproduce the result from the Fermi's golden rule. The calculation can be further simplified by only considering the CHCC (Auger-1) process which is predominant in the n-type material.

As a final note, the screened atomic potentials we employed in calculating the electronic structures of HgCdTe, InAsSb and InGaAs have been obtained by fitting the band energy values to the experimental data measured at 300 K. When investigating the material properties at different temperatures, we followed the common practice[8] in which the composition ratio of the ternary alloy is slightly changed to make its energy gap have the same value as what is predicted by the empirical formulas.[31,32] Since the quasi-Fermi level, which determines the statistical factors and self-energies in Eqs. (1), (10), and (13), is directly related to the band gap energy, this change is essential to incorporate all the important temperature effects in the calculation.

III. RESULTS

A. Model comparison

First, we calculated the direct Auger recombination lifetime in $Hg_{0.78}Cd_{0.22}Te$ and compared the obtained values with other theoretical calculations and the BLB formula. Fig. 1 shows the temperature dependence of the minority carrier lifetime due to direct Auger process. In the figure, solid lines represent the results from this work, circle symbols show the 14-band $k \cdot p$ results from Grein *et al.*,[9] dashed lines give the calculation results of Bertazzi *et al.*,[10] and dashed-dotted lines are from BLB formula. An overlap integral factor $|F_1F_2| = 0.16$ is used in the BLB formula to best fit to the numerical results.

As is shown, the three full band numerical results agree well with each other in the high temperature range while at low temperatures some differences appeared between Grein's result and the one from this work. We argue that the differences may come from the details of the band structures used in these works. At high temperatures, since more electrons and holes present in the bands, the available Auger recombination final states are abundant making the contribution from each transition smaller. As a result, the impact of the band structure details, especially the states close to the band edge, on the total recombination rate reduced. On the contrary, at low temperatures, due to the fact that most of the electrons and holes are concentrated at the band edge, very few direct recombination paths can fulfill both momentum and energy conservation in the Auger process. This results in a total direct recombination rate that is sensitive to the nature of the involving energy values and wavefunctions. Since both this work and Bertazzi's calculation used the same EPM band, but a different formulation for the self-energy, the calculated carrier lifetime agrees better with each other, comparing to the one from the $k \cdot p$ bands. Similar behavior

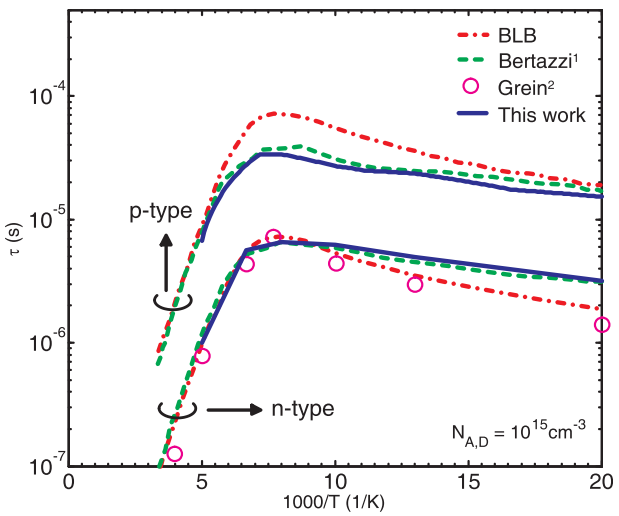

FIG. 1. Calculated temperature dependence of direct Auger recombination lifetime in $Hg_{0.78}Cd_{0.22}Te$ from Green's function theory (solid lines), 1: Bertazzi's work[10] (dashed lines), 2: Grein's work[9] (circles), and BLB formula with $|F_1F_2| = 0.16$ (dashed-dotted lines). The upper group of curves represents the results for p-type material (CHLH, Auger-7 process), while the lower group is for n-type material. The doping concentration in both cases is $10^{15}\,cm^{-3}$.

can also be observed in the calculated hole lifetime which is shown in the upper group of curves. Furthermore, though not shown in the figure, the PA indirect contribution to the Auger recombination is also calculated along with the direct part and is found to be small compared to the direct process. In fact at 200 K, the difference between direct and total (direct + PA indirect) Auger lifetime is less than 7% which is within the error of the Monte-Carlo integration techniques. Comparing the numerical results to the BLB formula, it is obvious that the difference between numerical results and BLB values is larger at low temperature, which suggests that it may be necessary to use a temperature-dependent $|F_1F_2|$ in the BLB formula to fully reproduce the numerical results. Indeed, the overlap integral factor actually represents the coupling of the four Bloch states in the Auger process, which will definitely change with the temperature through the change of the band gap energy. Consequently, it is of great importance to understand the temperature dependence of $|F_1F_2|$ in order to use the BLB formula effectively and accurately.

B. Minority carrier lifetime in *n*-type $InAs_{0.91}Sb_{0.09}$ and $Hg_{0.67}Cd_{0.33}Te$

One of the III-V materials emerging as a possible competitor to HgCdTe and InSb in the MWIR is $InAs_{1-x}Sb_x$. Among all the compositions in the $0 < x < 1$ range, the LM $InAs_{0.91}Sb_{0.09}$/GaSb system is of great importance due to the possibility of growing high quality barrier detector structures and type-2 superlattices (T2SL).

In this section, we investigated the radiative and Auger recombination lifetime in n-type $InAs_{0.91}Sb_{0.09}$ and compared it to the corresponding values for $Hg_{0.67}Cd_{0.33}Te$, since both of them have a cutoff wavelength of 4 μm at 200 K. The calculated radiative and Auger recombination rates are presented as a function of lattice temperature and doping concentration in Figs. 2(a) and 2(b), respectively.

As can be seen in Fig. 2(a), though diminishing at higher doping concentration, the PA indirect Auger process contributes a large portion to the total Auger recombination lifetime in $Hg_{0.67}Cd_{0.33}Te$ over the doping range from $10^{14}\,cm^{-3}$ to $5 \times 10^{16}\,cm^{-3}$. In fact, at $N_D = 10^{14}\,cm^{-3}$, the indirect Auger rate is twice as large as the direct Auger rate, whereas at $N_D = 10^{16}\,cm^{-3}$ the two processes almost contribute equally to the total recombination rate. In the case of $InAs_{0.91}Sb_{0.09}$, the relative strength of indirect Auger to the direct Auger is smaller and it can be seen that at high doping concentration, the contribution from the indirect process almost vanished. This variation of the relative strength between direct and indirect Auger rate with the doping concentration can be qualitatively explained by considering the available recombination paths. As was stated above, the low probability of indirect Auger process can actually be compensated by the large availability of final states in k-space. When the doping concentration is low, carriers tend to occupy the states at the band edge where the available direct recombination path is limited. As to indirect processes, with the assistance of phonon scattering carriers can first be scattered to a state far from the band edge and recombines with the final states that

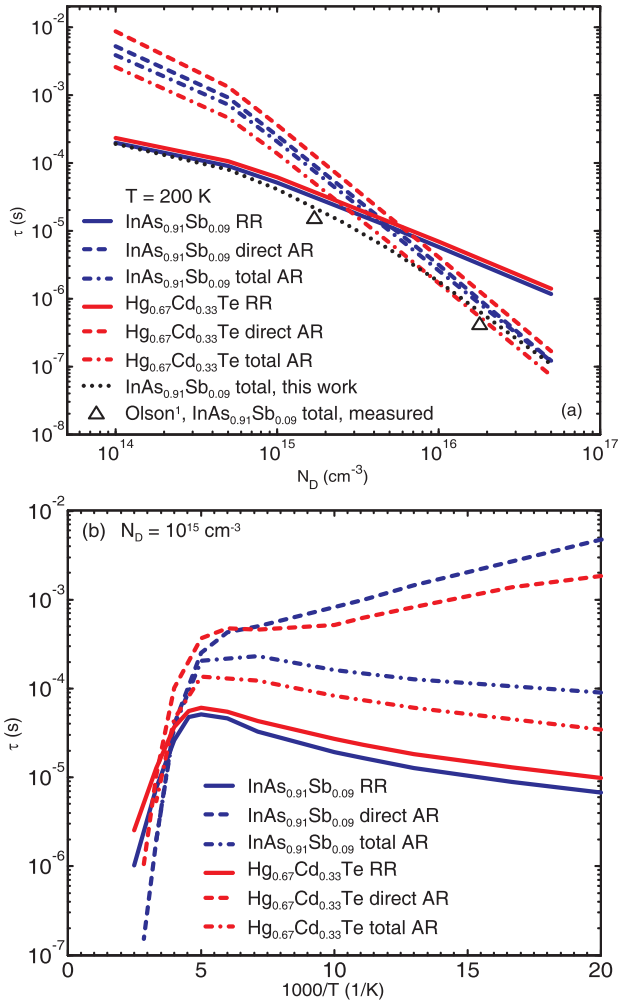

FIG. 2. Calculated radiative (solid lines), direct (dashed lines), and PA indirect (dashed-dotted lines) Auger recombination lifetime as a function of (a) *n*-type doping concentration and (b) lattice temperature for $InAs_{0.91}Sb_{0.09}$ (blue lines) and $Hg_{0.67}Cd_{0.33}Te$ (red lines). A lattice temperature of 200 K is assumed in (a) while a doping of $N_D = 10^{15}\,cm^{-3}$ is used in (b). The dotted line in (a) is the total lifetime (Auger and radiative lifetime) for $InAs_{0.91}Sb_{0.09}$ at 200 K. For comparison, the open triangles show the experimental values measured by 1: Olson and coworkers.[33]

fulfills both energy and momentum conservation. Since the number of final states in this case is usually abundant, the total recombination rate therefore increases. Consequently, as the direct process is limited by the available final states, the indirect process becomes more important at low doping level. A similar analysis can also be applied to the case of high doping concentrations, where more carriers will present in higher energy states, effectively increasing the available direct recombination paths. Due to its larger interaction strength, the direct process, as a result, dominates over the indirect process.

We further compared the Auger recombination lifetime with the radiative lifetime. As is expected, when the doping concentration is higher than $3 \times 10^{15}\,cm^{-3}$ for $Hg_{0.67}Cd_{0.33}Te$ or $5 \times 10^{15}\,cm^{-3}$ for $InAs_{0.91}Sb_{0.09}$, the minority carrier lifetime is dominated by the Auger process whereas at lower doping concentration, the radiative recombination is found to be the limiting factor. From Fig. 2(a), it can be seen that although the lifetime difference is not very significant, $InAs_{0.91}Sb_{0.09}$ has better intrinsic minority carrier lifetime at high doping concentrations thanks to its smaller total Auger recombination rate.

In Fig. 2(a), the total lifetime (combined Auger and radiative) calculated for $InAs_{0.91}Sb_{0.09}$ at 200 K is also compared to the experimental data from Olson and coworkers[33] that measured the carrier lifetime in bulk $InAs_{0.91}Sb_{0.09}$ at different temperatures and doping concentrations. It can be seen that the calculated values are in good agreement with the measured data which indicates that the intrinsic recombination mechanisms are indeed the limiting factors in determining the carrier lifetime in the material. Indeed, from Olson's reported data pertinent to unintentionally doped and doped bulk $InAs_{0.91}Sb_{0.09}$, one can evince that SRH recombination, although present, is not dominant. On the contrary, in the case of T2SL SRH recombination is the determining factor of the carrier lifetime below 200 K.

The calculated temperature-dependent hole lifetimes in the two alloys are presented in Fig. 2(b) where radiative, direct, and total Auger processes are compared at a constant *n*-type doping of $10^{15}\,cm^{-3}$. Although it may seem counterintuitive, the results show that the contribution from the PA indirect Auger process to the total Auger rate actually becomes larger at lower temperature when the average number of phonon decreased. This phenomenon, however, can be understood by considering the two competing factors in determining the PA process: the strength of the recombination and the final states available for the recombination process.

The strength of the PA Auger recombination, which is related to the matrix element for Auger process and band broadening, decreases at lower temperature due to the diminishing phonon population. Indeed, further calculation of the self energy confirmed that the broadening of the band under the phonon perturbation decreases with the temperature. However, it also should be noted that from Eq. (13) the broadening of the bands will converge to a finite value as the temperature approaches zero. In fact, if one sets the phonon population factor $P(\hbar\omega)$ to zero and the electron population factor to 1 or 0 depending on the value of the energy E, the band broadening $\mathrm{Im}\Sigma(\mathbf{k},E)$ always exists through the emission of optical phonons which, unlike phonon absorption, does not require the presence of a phonon population. As a result, the PA process will always contribute to the total Auger recombination even at extremely low temperature.[34]

The other factor that will affect the total PA Auger rate is the number of available final states for Auger recombination. As the temperature decreases, carriers will tend to concentrate at the band edge. This in turn reduces the available direct recombination final states that fulfill both energy and momentum conservation. On the other hand, through the emission/absorption of a phonon, the momentum conservation among the four electron states can be relaxed with the phonon providing the additional momentum. Therefore, the number of available final states for PA Auger process increases. Moreover, in order to have a meaningful comparison between different materials that may have different dopant activation energies, the carrier concentration is kept fixed for all the temperatures investigated (no freeze-out effect is

included). This means that, in order to maintain the same amount of electrons and holes in the conduction and valence band, the Fermi level moves closer to the band edges at lower temperature. As a result, the statistical factor for electron $\Theta(E)$ is found to be higher at lower temperature when evaluating at the conduction band edge. Same effect is also true for the hole distribution. Consequently, even though the strength of the PA process diminishes at low temperature, the total PA Auger rate slightly increases when the temperature changes from 200 K to 50 K for MWIR materials. Further calculation at 10 K gives a much lower total Auger rate indicating that the rate of PA process will eventually decrease at temperature below 50 K.

It should be noted that even though the indirect Auger dominates over the direct Auger process at low temperature, the minority carrier lifetime in this range is limited by the radiative recombination. Indeed, when the temperature becomes lower than 250 K, the radiative recombination becomes stronger than the total Auger recombination in both materials with the $Hg_{0.67}Cd_{0.33}Te$ having larger overall lifetime. In the high temperature range, due to the fact that more carriers now have enough energy to occupy high energy states, the direct process gradually contributes to all of the Auger recombination events, and eventually exceeds the radiative process and becomes the limiting factor of the hole lifetime in the two materials. It is also worth noting that for all the temperatures considered here $Hg_{0.67}Cd_{0.33}Te$ generally has slightly better intrinsic minority carrier lifetime than $InAs_{0.91}Sb_{0.09}$ because of its larger radiative lifetime at low temperature as well as weaker direct Auger recombination rate at high temperature.

As a final remark, we want to emphasize that the calculations presented in this work do not include the effect of photon recycling (PR), which tends to increase the radiative recombination lifetime extracted from devices level measurements. In fact, earlier work on PR in HgCdTe,[35,36] indicated that the enhancement of the radiative lifetime due to PR can be as high as 25 times which may explain why in some cases the calculated lifetime are lower than the reported values for MWIR HgCdTe.[37] However, as the derivation in Ref. 35 suggests, the effect of PR largely depends on the geometry of the devices such as the thickness of the layers and the shape of the device boundaries which can vary significantly from device to device. For these reasons, the aim of the present work is to provide a baseline evaluation of the radiative recombination lifetime in materials under the assumption that PR effect can be ignored. This is obviously the worst case scenario in which the lifetime is not enhanced by the PR effect.

The corresponding Auger-1 coefficients calculated from Eq. (7) are shown in Fig. 3. Depending on the recombination mechanisms used in the calculation, the total Auger coefficients, which consist of both phonon-assisted ($C_{n,ph}$) and direct (C_{n0}) Auger processes, are plotted alongside the direct Auger coefficients as a function of temperature. As can be seen, at high temperature range ($T > 200$ K) when both materials become nearly intrinsic, the total Auger coefficient almost remains constant at 4.8×10^{-27} cm^6/s and 3.7×10^{-27} cm^6/s for $Hg_{0.67}Cd_{0.33}Te$ and $InAs_{0.91}Sb_{0.09}$,

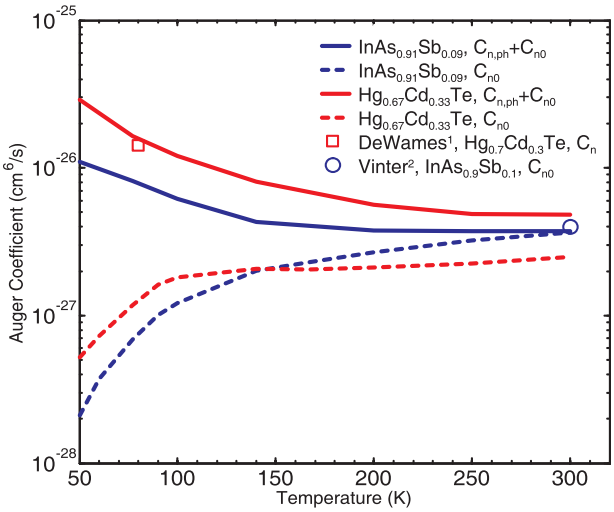

FIG. 3. Temperature dependence of Auger-1 coefficients for $InAs_{0.91}Sb_{0.09}$ (blue lines) and $Hg_{0.67}Cd_{0.33}Te$ (red lines) is compared with 1 (square): fitted C_n of $Hg_{0.7}Cd_{0.3}Te$ at 80 K from DeWames's work,[38] and 2 (circle): calculated direct Auger coefficient C_{n0} in $InAs_{0.9}Sb_{0.1}$ at 300 K.[15] The solid lines here represent the total Auger coefficients (PA indirect + direct), and the dashed lines are computed from the direct Auger process only.

respectively. The PA indirect Auger process in this temperature range does not provide a significant contribution to the total Auger rate as opposed to what happens at lower temperatures. For example, in the case of $InAs_{0.91}Sb_{0.09}$, the direct Auger coefficient almost equals to the total one at 300 K which also agrees with Vinter's calculation (circle).[15] However, as the temperature decreases, the PA indirect Auger process becomes increasingly important as the direct Auger coefficient drops while the total Auger coefficient, on the contrary, increases. The square symbol in the figure shows the value of the fitted Auger coefficient for $Hg_{0.7}Cd_{0.3}Te$ from the experimental data with a donor concentration of 10^{15} cm^{-3} obtained by DeWames *et al.*[38] We found that to reproduce the experimental value it is necessary to include the contribution of the indirect Auger process, since the direct Auger coefficient at 80 K is one order of magnitude lower than the measured data. Adding the indirect Auger process to the calculation leads to a much better agreement between the calculated and measured total Auger coefficient, and we believe that the small remaining differences between them comes from small alloy composition differences and numerical errors.

C. Minority carrier lifetime in *n*-type $In_{0.53}Ga_{0.47}As$ and $Hg_{0.38}Cd_{0.62}Te$

Radiative and Auger recombination lifetimes in $In_{0.53}Ga_{0.47}As$ and $Hg_{0.38}Cd_{0.62}Te$ which have a cutoff wavelength of 1.6 μm at 300 K are presented in Figs. 4(a) and 4(b). Unlike $Hg_{0.38}Cd_{0.62}Te$ in which the contribution from the PA indirect Auger recombination accounts for about 83% of the total Auger rate at 300 K, the indirect Auger process in $In_{0.53}Ga_{0.47}As$ shown in Fig. 4(a) is very weak and the two lines representing its total Auger lifetime and the lifetime due to direct Auger process almost overlap. As opposed to MWIR materials, the dominant recombination

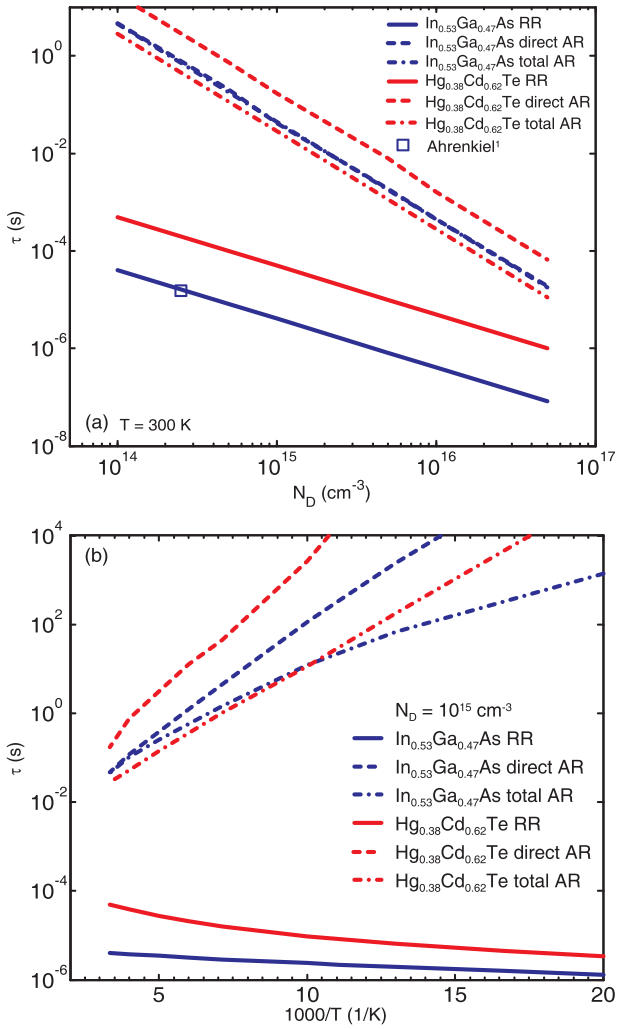

FIG. 4. Radiative (solid lines), direct (dashed lines), and PA indirect (dashed-dotted lines) Auger recombination lifetime is computed as a function of (a) n-type doping concentration and (b) lattice temperature for $In_{0.53}Ga_{0.47}As$ (blue lines) and $Hg_{0.38}Cd_{0.62}Te$ (red lines). 300 K is assumed in the calculation of (a) while an n-type doping of $N_D = 10^{15}\,cm^{-3}$ is used in (b). In (a), the lifetime measured in $In_{0.53}Ga_{0.47}As$ at low-injection from 1: Ref. 39 is labeled as square.

process for the two SWIR materials in the doping range from $10^{14}\,cm^{-3}$ to $5\times10^{16}\,cm^{-3}$ is always the radiative recombination, and we found that the calculated radiative recombination lifetime indeed matches very well with the measured lifetime in the case of $In_{0.53}Ga_{0.47}As$ (square symbol).[39] Furthermore, by extrapolating the calculated curve of $In_{0.53}Ga_{0.47}As$ to higher doping concentrations, we find that an intersection between the total Auger lifetime and radiative lifetime occurs around a doping concentration of $5\times10^{18}\,cm^{-3}$, which also agrees with the measurement done by Ahrenkiel *et al.*[39] We notice that even though the Auger lifetime in the two SWIR materials are similar, due to the large radiative lifetime in $Hg_{0.38}Cd_{0.62}Te$ and the high intersection point between Auger and radiative process, the overall intrinsic minority carrier lifetime in $Hg_{0.38}Cd_{0.62}Te$ outperforms that in the $In_{0.53}Ga_{0.47}As$ by large amount within the investigated doping range.

The temperature dependence of the two recombination processes in SWIR materials is shown in Fig. 4(b). As can be seen, the Auger lifetime, including both direct Auger and PA indirect Auger processes, increases dramatically as the temperature decreases which is different from what was found in MWIR and LWIR materials. In fact, as the band gap of the material increases, the available final states in the band structures decrease, leading to a weaker Auger recombination regardless of the assistance from the phonons. It is obvious that from 300 K to 50 K, the dominant recombination process for the two materials is still the radiative process with the $Hg_{0.38}Cd_{0.62}Te$ having longer carrier lifetime.

The Auger coefficients calculated from the total Auger-1 lifetime of the two SWIR materials are presented in Fig. 5. Although the PA indirect Auger process here also contributes substantially to the total Auger coefficient at low temperatures, the calculated total Auger coefficient $C_{n,ph}+C_{n0}$, in contrast to the MWIR material, drops fast as the temperature decreases. In this figure, the measurement done by Ahrenkiel *et al.*[39] for $In_{0.53}Ga_{0.47}As$ at 300 K, averaged over n-type and p-type materials, is reported in the form of triangle, whereas an early theoretical calculation using density functional theory (DFT) for direct Auger process is shown as circle symbol.[40] The square symbol is the calculated Auger coefficient C_p due to CHSH process (Auger-S) from our numerical model. It can be seen that, although the measured $C_{n,p}$ is about three times larger than our numerical results C_n for n-type material, by taking the C_p into consideration our calculated value agrees with Ahrenkiel's measurement within a reasonable error. In fact, using the measured lifetime in the sample with $N_A = 2\times10^{19}\,cm^{-3}$ from Ref. 39, we estimate a C_p of $1\times10^{-28}cm^6/s$ which is very close to the C_p from our calculation, that is $1.08\times10^{-28}cm^6/s$. A relatively good agreement is also found between the numerical direct Auger coefficient C_{n0} from our model and Picozzi's theoretical calculation. Finally, we want to point out that although the PA indirect Auger process diminished at high temperature in

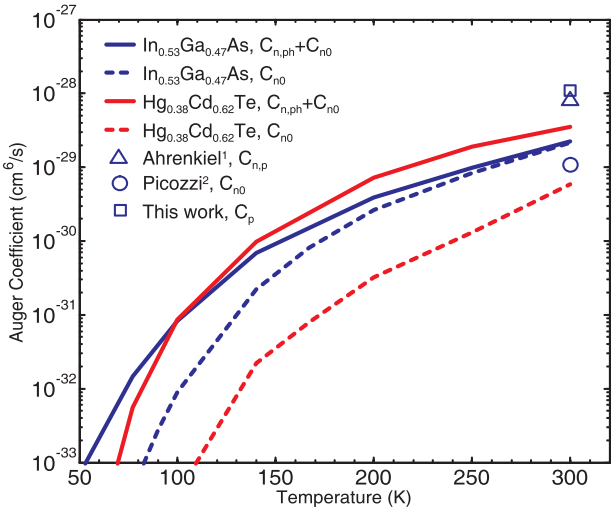

FIG. 5. Temperature dependence of Auger-1 coefficient for $In_{0.53}Ga_{0.47}As$ (blue lines) and $Hg_{0.38}Cd_{0.62}Te$ (red lines) is compared with 1: fitted $C_{n,p}$ of $In_{0.53}Ga_{0.47}As$ at 300 K from the measured data,[39] and 2: calculated direct Auger coefficient C_{n0} of $In_{0.53}Ga_{0.47}As$.[40] The solid lines here represent the total Auger coefficient (PA indirect + direct), and the dashed lines are computed from the direct Auger process only. The Auger coefficient C_p due to CHSH process from this work is labeled as square.

$In_{0.53}Ga_{0.47}As$, it is still important in $Hg_{0.38}Cd_{0.62}Te$. In fact, the direct Auger coefficient at this temperature is obviously lower than the total coefficient which has been reported in both Figs. 4(b) and 5.

D. $|F_1F_2|$ for MWIR and SWIR materials

In order to facilitate the use of BLB formula in calculating the Auger coefficients, we put the calculated overall Auger-1 coefficient back into Eq. (9) and evaluated the corresponding overlap integral factor $|F_1F_2|$ which is plotted in Fig. 6. As can be noticed, for the MWIR materials the values of $|F_1F_2|$ for $InAs_{0.91}Sb_{0.09}$ and $Hg_{0.67}Cd_{0.33}Te$ do not change significantly in the temperature range between 100 K and 300 K in which their values are 0.07–0.085 and 0.1–0.125, respectively. As to the SWIR materials, due to the much weaker Auger recombination at low temperature, the calculated factors $|F_1F_2|$ vary significantly between 100 K and 300 K, with their values spanning the range 0.04–0.07 for $In_{0.53}Ga_{0.47}As$ and 0.005–0.035 for $Hg_{0.38}Cd_{0.62}Te$.

In the low temperature regime, when $T < 100$ K, $|F_1F_2|$ for all the four materials changes significantly with the temperature and we speculated that it is probably caused by the assumption of non-degenerate material approximation used in the BLB formula. In fact, the Boltzmann distribution can only approximate the Fermi-Dirac distribution in the limit of non-degenerate situation which is reasonable at high temperature. In the low temperature range, the distribution of carriers is governed by the Pauli exclusion principle and the use of Boltzmann statistic would lead to an un-physical increase of the overlap factor as is the case in Fig. 6. Although the BLB formula becomes inaccurate at low temperature, it is still a quick way to estimate the Auger coefficient and lifetime in the context of device simulation as long as the $|F_1F_2|$ factor is selected carefully. However, instead of choosing the overlap factor between 0.1 and 0.3 as a common practice, for example, in $Hg_{0.78}Cd_{0.22}Te$ a $|F_1F_2| = 0.16$ gives good results from BLB formula, we found that for MWIR material a proper $|F_1F_2|$ usually lies around 0.1 whereas for SWIR material, $|F_1F_2|$ is always below 0.1 and varies drastically with temperature. Indeed, as the band gap of material increases, the interaction between the electronic states that are involved in the Auger recombination process becomes weaker, which in turn leads to a smaller $|F_1F_2|$.

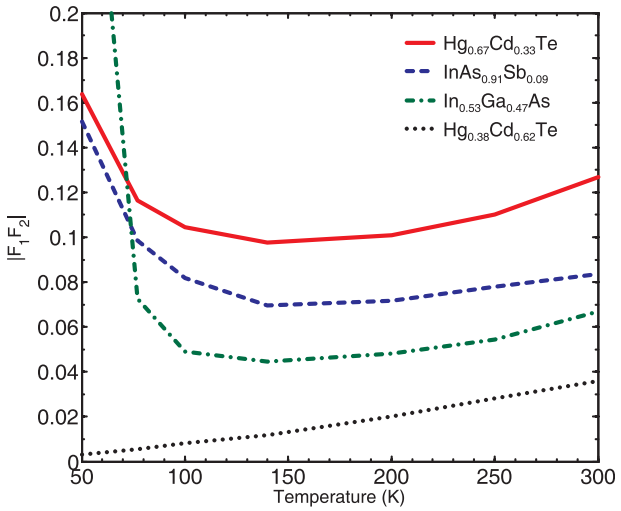

FIG. 6. Overlap integral factors $|F_1F_2|$ for $Hg_{0.67}Cd_{0.33}Te$ (solid line), $InAs_{0.91}Sb_{0.09}$ (dashed line), $In_{0.53}Ga_{0.47}As$ (dashed-dotted line), and $Hg_{0.38}Cd_{0.62}Te$ (dotted line) are calculated as a function of temperature using the BLB formula in Eq. (9) and the numerical Auger-1 coefficient $C_{n,ph} + C_{n0}$ from this work.

To conclude this section, we want to point out that in the original derivation of BLB formula,[23] only the pure collision mechanism is taken into account. However, in our calculation, both pure collision and PA Auger process are considered. As a result, the overlap factor values that we derive are larger than the ones computed by Krishnamurthy *et al.*[8] who followed the same calculation procedure as that proposed by Beattie and Landsberg.

IV. CONCLUSION

We have calculated and compared the doping-dependent and temperature-dependent radiative and Auger recombination lifetime, as well as the corresponding Auger coefficients, in the *n*-type HgCdTe, InAsSb, and InGaAs intended for operation in the MWIR and SWIR spectral bands. Using the Green's function theory and EPM full band structures, both direct and PA indirect Auger processes are included in the numerical calculation which is implemented through the Monte-Carlo integration method. Our results indicate that for $InAs_{0.91}Sb_{0.09}$ ($Hg_{0.67}Cd_{0.33}Te$), when the *n*-doping concentration is greater than $5 \times 10^{15}\,cm^{-3}$ ($3 \times 10^{15}\,cm^{-3}$) the Auger process dominates over the radiative process whereas, at $T < 250$ K, the radiative process becomes the limiting factor for the intrinsic minority carrier lifetime in both materials. Comparing the two materials for the MWIR band, we find that $Hg_{0.67}Cd_{0.33}Te$ generally has slightly better intrinsic minority carrier lifetime over $InAs_{0.91}Sb_{0.09}$ in the temperature range of 50 K to 300 K due to its larger radiative lifetime at low temperature as well as weaker direct Auger recombination rate at high temperature.

For SWIR materials, namely, $In_{0.53}Ga_{0.47}As$ and $Hg_{0.38}Cd_{0.62}Te$, our calculations indicate that over the *n*-type doping from $10^{14}\,cm^{-3}$ to $5 \times 10^{16}\,cm^{-3}$ and temperature between 50 K and 300 K, the radiative recombination process always dominates over the Auger process which is more than three orders of magnitude weaker than that in MWIR materials. Moreover, the results also suggest that $Hg_{0.38}Cd_{0.62}Te$ has a better intrinsic minority carrier lifetime compared with $In_{0.53}Ga_{0.47}As$ due to its lower radiative recombination rate.

Furthermore, the estimation of the overlap integral factor $|F_1F_2|$, which is evaluated by matching the BLB formula to our numerical results, shows that for MWIR materials, $|F_1F_2|$ usually lies around 0.1 and does not change much within the temperature between 100 K and 300 K. Specifically, for $InAs_{0.91}Sb_{0.09}$ and $Hg_{0.67}Cd_{0.33}Te$ $|F_1F_2|$ is found to be 0.07–0.085 and 0.1–0.125, respectively. In the case of SWIR materials, $|F_1F_2|$ is always below 0.1 and varies significantly with temperature.

Overall, our calculations unveil the importance of PA indirect Auger process in determining the total intrinsic

minority carrier lifetime in MWIR and SWIR materials, which will further benefit the simulation of dark current, internal quantum efficiency, and detectivity in the design of IR detectors.

ACKNOWLEDGMENTS

The authors wish to thank Professor F. Bertazzi for his help in understanding the many subtleties of the numerical model. We are grateful to Dr. R. DeWames for his many useful comments. Funding for this work was provided by the U.S. Army Research Laboratory through the Collaborative Research Alliance (CRA) for MultiScale multidisciplinary Modeling of Electronic materials (MSME).

[1]P. Klipstein, O. Klin, S. Grossman, N. Snapi, B. Yaakobovitz, M. Brumer, I. Lukomsky, D. Aronov, M. Yassen, B. Yofis, A. Glozman, T. Fishman, E. Berkowicz, O. Magen, I. Shtrichman, and E. Weiss, Proc. SPIE **7660**, 76602Y (2010).
[2]A. I. D'Souza, A. C. Ionescu, M. Salcido, E. Robinson, L. Dawson, and D. L. Okerlund, Proc. SPIE **8012**, 80122S (2011).
[3]J. Schuster, C. A. Keasler, M. Reine, and E. Bellotti, J. Electron. Mater. **41**, 2981 (2012).
[4]C. A. Keasler and E. Bellotti, Appl. Phys. Lett. **99**, 091109 (2011).
[5]J. Schuster and E. Bellotti, Appl. Phys. Lett. **101**, 261118 (2012).
[6]J. Schuster and E. Bellotti, Opt. Express **21**, 14712 (2013).
[7]D. Edwall, R. E. Dewames, W. V. Mclevige, J. G. Pasko, and J. M. Arias, J. Electron. Mater. **27**, 698 (1998).
[8]S. Krishnamurthy, M. Berding, and Z. Yu, J. Electron. Mater. **35**, 1369 (2006).
[9]C. H. Grein, M. E. Flatte, and Y. Chang, J. Electron. Mater. **37**, 1415 (2008).
[10]F. Bertazzi, M. Goano, and E. Bellotti, J. Electron. Mater. **40**, 1663 (2011).
[11]J. R. Lindle, J. R. Meyer, C. A. Hoffman, and F. J. Bartoli, Appl. Phys. Lett. **67**, 3153 (1995).
[12]J. R. Meyer, C. L. Felix, W. W. Bewley, I. Vurgaftman, E. H. Aifer, L. J. Olafsen, J. R. Lindle, C. A. Hoffman, M.-J. Yang, B. R. Bennett, and B. V. Shanabrook, Appl. Phys. Lett. **73**, 2857 (1998).
[13]E. H. Steenbergen, B. C. Connelly, G. D. Metcalfe, H. Shen, M. Wraback, D. Lubyshev, Y. Qiu, J. M. Fastenau, A. W. K. Liu, S. Elhamri, O. O. Cellek, and Y.-H. Zhang, Appl. Phys. Lett. **99**, 251110 (2011).
[14]C. H. Grein, P. M. Young, M. E. Flatté, and H. Ehrenreich, J. Appl. Phys. **78**, 7143 (1995).
[15]B. Vinter, Phys. Rev. B **66**, 045324 (2002).
[16]W. Bardyszewski and D. Yevick, J. Appl. Phys. **58**, 2713 (1985).
[17]M. Takeshima, Phys. Rev. B **25**, 5390 (1982).
[18]M. Takeshima, Jpn. J. Appl. Phys., Part 1 **23**, 428 (1984).
[19]H. Wen and E. Bellotti, J. Electron. Mater. **43**, 2841 (2014).
[20]H. Wen and E. Bellotti, Phys. Rev. B **91**, 035307 (2015).
[21]D. B. Laks and G. F. Neumark, Phys. Rev. B **42**, 5176 (1990).
[22]D. Harrison, R. A. Abram, and S. Brand, J. Appl. Phys. **85**, 8178 (1999).
[23]A. R. Beattie and P. T. Landsberg, Proc. R. Soc. London, Ser. A **249**, 16 (1959).
[24]S. Krishnamurthy, A. Sher, and A.-B. Chen, J. Appl. Phys. **82**, 5540 (1997).
[25]J. Bude, N. Sano, and A. Yoshii, Phys. Rev. B **45**, 5848 (1992).
[26]J. P. Walter and M. L. Cohen, Phys. Rev. B **5**, 3101 (1972).
[27]E. Bellotti and D. D'Orsogna, IEEE J. Quantum Elect. **42**, 418 (2006).
[28]V. C. Lopes, A. J. Syllaios, and M. C. Chen, Semicond. Sci. Technol. **8**, 824 (1993).
[29]See http://www.ioffe.ru/SVA/NSM/Semicond/index.html for Ioffe.
[30]G. D. Mahan, *Many-Particle Physics*, 2nd ed. (Plenum Press, New York, USA, 1993).
[31]A. Rogalski, *New Ternary Alloy Systems for Infrared Detectors* (SPIE, The International Society for Optical Engineering, 1994).
[32]P. Capper, *Properties of Narrow Gap Cadmium-Based Compounds* (INSPEC, IEE, London, UK, 1994).
[33]B. V. Olson, E. A. Shaner, J. K. Kim, J. F. Klem, S. D. Hawkins, M. E. Flatté, and T. F. Boggess, J. Appl. Phys. **103**, 052106 (2013).
[34]E. Kioupakis, P. Rinke, K. T. Delaney, and C. G. V. de Walle, Appl. Phys. Lett. **98**, 161107 (2011).
[35]R. G. Humphreys, Infrared Phys. **23**, 171 (1983).
[36]C. H. Grein, H. Ehrenreich, and E. Runge, Proc. SPIE **2999**, 277 (1997).
[37]M. A. Kinch, *Fundamentals of Infrared Detector Materials* (SPIE Press, 2007).
[38]R. DeWames, P. Maloney, C. Billman, and J. Pellegrino, Proc. SPIE **8012**, 801239 (2011).
[39]R. K. Ahrenkiel, R. Ellingson, S. Johnston, and M. Wanlass, Appl. Phys. Lett. **72**, 3470 (1998).
[40]S. Picozzi, Phys. Rev. Lett. **89**, 197601 (2002).